

Recent Advances in Digital Longitudinal Monitoring of Fiber-Optic Link

Takeo Sasai, Minami Takahashi, Runa Kaneko, Yoshiaki Sone, Masanori Nakamura, and Etsushi Yamazaki

NTT Network Innovation Laboratories, NTT, 1-1 Hikari-no-oka, Yokosuka, Kanagawa, 239-0847 Japan

takeo.sasai@ntt.com

Abstract: We review digital longitudinal monitoring, particularly longitudinal power monitoring (LPM), which estimates fiber-longitudinal optical power at a coherent receiver. We highlight key experiments including precise LPM closely matching OTDR and its feasibility demonstration at operational powers. © 2024 The Author(s)

1. Introduction

Optical networks are becoming increasingly complex due to trends such as disaggregation, dynamic provisioning and routing, and ultra-wideband transmission. To fully leverage the potential capacity and maintain these advanced networks efficiently, it is crucial for operators to monitor the physical parameters the entire link, including optical power and locations of loss anomalies.

Digital longitudinal monitoring (DLM), which has been studied intensively recently, estimates various physical link parameters distributed in the *fiber-longitudinal* direction solely by processing signals received at a digital coherent receiver. Demonstrated monitored parameters include the longitudinal optical power profile [1-8], span-wise chromatic dispersion (CD) map [2], amplifiers' gain tilt [2, 8], optical filter detuning [2], polarization dependent loss [9-11], and multi-path interference [6]. DLM enables the localization of multiple anomalies over multi-span links without the need for dedicated hardware devices such as optical time domain reflectometers (OTDR) and optical spectrum analyzers, thereby reducing operational costs. Among the monitored parameters, the longitudinal power monitoring (LPM) is of particular importance since optical power determines the generalized signal-to-noise ratio and its distributed measurement allows the localization of loss anomaly, both of which facilitate network management and control. Various demonstrations of LPM have showcased its capabilities, including a precise LPM closely matching OTDR [4], demonstrations over 10,000 km [5], and LPM using commercial transponders [7, 13].

The primary challenge of DLM is that it relies on the fiber nonlinearity and high fiber launch power is desirable to achieve a sufficient accuracy, which causes a QoT degradation in adjacent WDM channels due to excessive nonlinear interference (NLI). Most previous demonstrations have adopted an optical power far higher than the operational point. We have recently demonstrated LPM under a system optimal launch power and WDM conditions with an accuracy enough to locate a 0.80 dB loss anomaly, demonstrating its feasibility of LPM for use in operations [4].

In this paper, we review the fundamentals and recent advancements in DLM, with a particular focus on LPM, including the localization principle, an inherent limitation on spatial resolution, algorithms, several key demonstrations, and future direction towards practical deployment of DLM. The demonstrations include a precise estimation with an RMS error of 0.18 dB from OTDR and LPM at system operational launch power [4].

2. Localization principle

LPM estimates the fiber-longitudinal optical power $P(z)$ from received waveforms by extracting the nonlinear phase shift $\gamma'(z) = \gamma(z)P(z)$ that the signals experienced during the fiber transmission, where $\gamma(z)$ is the fiber nonlinear coefficient at position z . The key mechanism for the localization of the optical power is the interaction between fiber nonlinearity and CD in optical fibers [3]. To elucidate the localization principle, let us consider the regular perturbation model for the fiber nonlinear propagation. In the first-order regular perturbation, the additive NLI $j\gamma'(z)|\mathbf{A}(z)|^2\mathbf{A}(z)$ is excited at each position on fibers, which is dependent on the original signal waveform $\mathbf{A}(z)$ (see Fig. 1). Such local NLIs propagate to the receiver, undergoing the remaining CD \widehat{D}_{zL} from z to the link end L , and evolve as $\gamma'(z)\mathbf{g}(z)$, where

$$\mathbf{g}(z) = j\widehat{D}_{zL}[|\mathbf{A}(z)|^2\mathbf{A}(z)]. \quad (1)$$

The total NLI at the receiver is the accumulation of the received local NLIs and represented as

$$\mathbf{A}_1(L) = \int_0^L \gamma'(z)\mathbf{g}(z)dz \quad (2)$$

which shows $\{\mathbf{g}(z)\}_z$ form a basis of the total NLI. Two of these basis vectors $\mathbf{g}(z)$ and $\mathbf{g}(z + \Delta z)$ are linearly independent in the presence of sufficient CD over the distance Δz , allowing the corresponding coefficient $\gamma'(z)$ to be extracted at the receiver. The qualitative understanding is that sufficient CD alters the original signal waveforms during the propagation, and the excited NLIs at different locations are thus unique and distinguishable upon reception.

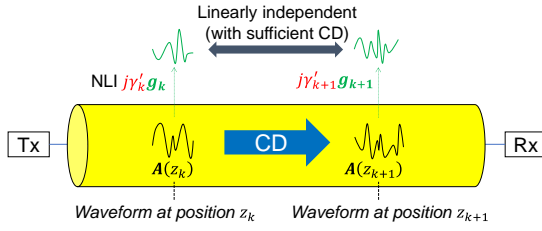


Fig. 1. Perturbation model of fiber nonlinear propagation. Nonlinear interferences (NLIs) from positions z_k and z_{k+1} are linearly independent with sufficient CD, allowing the estimation of $\gamma'_k = \gamma'(z_k)$.

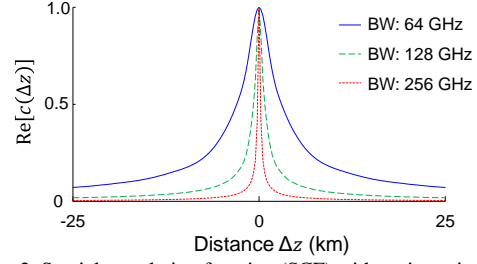


Fig. 2. Spatial correlation function (SCF) with various signal bandwidth. $\beta_2 = -20.5\text{ps}^2/\text{km}$ is assumed.

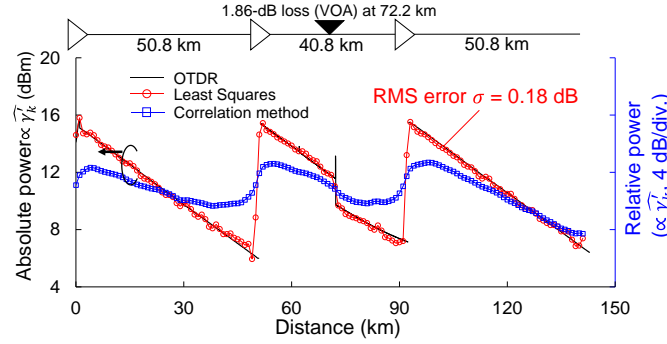


Fig. 3. Experimental results of LPM with least squares (red) and correlation method (blue) with 1.86-dB attenuation inserted at 72.2 km.

3. Spatial resolution

One straightforward approach to extract the expansion coefficient $\gamma'(z_k)$ at position z_k ($k \in [0, K-1]$) is to take the inner product of $\mathbf{A}_1(L)$ and the corresponding basis vector $\mathbf{g}_k = \mathbf{g}(z_k)$. However, the basis $\{\mathbf{g}(z)\}_z$ is not orthogonal: the resulting inner product $\mathbf{g}_k^\dagger \mathbf{A}_1(L)$ involves not only $\gamma'(z_k)$ but also ones at neighboring positions. In fact, it has been shown in [3] that the expectation of the inner product of two vectors $\mathbf{g}(z)^\dagger \mathbf{g}(z + \Delta z)$ is expressed under assumptions of stationary Gaussian signal and constant CD β_2 over the link with negligible high-order dispersions as:

$$c(\Delta z) \propto \frac{1}{\sqrt{1 + 2j\left(\frac{\Delta z}{z_{CD}}\right) + 3\left(\frac{\Delta z}{z_{CD}}\right)^2}} \quad (z_{CD} \approx \frac{0.288}{|\beta_2|BW^2} \text{ for Nyquist signals}) \quad (3)$$

which is called the spatial correlation function (SCF) or spatial response function [3, 6]. Here, BW is the signal bandwidth. Fig. 2 shows the SCF for various signal bandwidth BW. The SCF has a ‘width’ with long tails, suggesting that the estimated values of $\gamma'(z_k)$ contain contributions from neighboring positions. This means that there is an inherent uncertainty in determining the position of loss events, limiting the spatial resolution of LPM. The FWHM of the SCF is a good approximation of the SR, expressed as

$$SR \approx \frac{0.507}{|\beta_2|BW^2}, \quad (4)$$

implying that the spatial resolution is enhanced with a large CD and signal bandwidth [3].

4. Methods

The simple inner-product approach described above is called the correlation method (CM) [1, 6]. However, due to the non-orthogonality shown in the SCF, the entire output of CM $\mathbf{G}^\dagger \mathbf{A}_1 = [\mathbf{g}_0, \mathbf{g}_1, \dots, \mathbf{g}_{K-1}]^\dagger \mathbf{A}_1$ is expressed as the convolution of the true power profile and the SCF [3], which implies the sensitivity of the CM is limited as shown in Fig. 3 (blue). Another approach is the least squares (LS) $(\mathbf{G}^\dagger \mathbf{G})^{-1} \mathbf{G}^\dagger \mathbf{A}_1$ [4], which minimizes $\|\mathbf{G}\boldsymbol{\gamma}' - \mathbf{A}_1\|^2$. LS naturally deconvolves the convolution effects in CM by $(\mathbf{G}^\dagger \mathbf{G})^{-1}$, thereby achieving precise LPM as shown in red. However, the simple least squares suffers from instability related to the ill-posedness of LPM as pointed out in [4]. The penalized least squares was therefore used in [7] as

$$\hat{\boldsymbol{\gamma}}' = (\mathbf{G}^\dagger \mathbf{G} + \lambda \mathbf{I})^{-1} \mathbf{G}^\dagger \mathbf{A}_1, \quad (5)$$

where λ is a regularization parameter and \mathbf{I} is the identity matrix. This method generalizes CM and LS as it approaches CM for $\lambda \rightarrow \infty$ while it becomes LS for $\lambda = 0$.

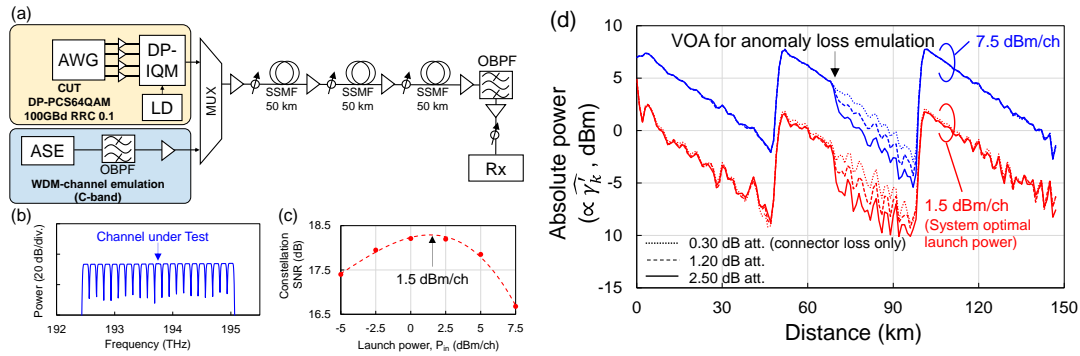


Fig. 4. (a) Experimental setup for WDM transmission. (b) Transmitted WDM spectra. (c) Constellation SNR as a function of fiber launch power. System optimal launch power was approximately 1.5 dBm/ch. (d) Experimental results of LPM under WDM conditions with various attenuation levels inserted.

Although most LPM demonstrations have utilized self-channel interference (SCI), cross-channel interference (XCI) or cross phase modulation can also be used to localize power events [14–16]. Although XCI-based methods require an access to two channels, they achieve high spatial resolution due to a large walk-off between two channels.

5. Experimental demonstrations

Fig. 3 shows a demonstration of LPM using the least squares estimation [4], which achieved the precise longitudinal once. The test used PCS 64QAM modulation with a roll-off factor of 0.1 and a symbol rate of 100 GBd. The link under test was a 142.4-km 3-span standard single mode fiber link with a 1.86-dB attenuation inserted at 72.2 km. The fiber launch power was set to 15 dBm/ch. While the CM (blue) reflects the overall power trend, it fails to align with OTDR and less sensitive to the loss anomaly, due to the convolution effect. On the other hand, the LS demonstrates a closer match with the OTDR, having an RMS error of 0.18 dB and a maximum absolute error of 0.57 dB. Fig. 4 shows the LPM experiment under the system optimal launch power and WDM conditions [4]. The WDM channels were loaded from an ASE source, shaped by an optical filter, with the channel under test set at the center of the WDM channels (Fig.4(a)(b)). The optimal power was around 1.5 dBm/ch (Fig.4(c)). As shown in Fig. 4(d), LPM shows a superior performance with high power (blue). However, the estimated power profiles at 1.5 dBm/ch are still clearly visible, enough to locate a loss anomaly. The RMS error from OTDR prior to the loss event was $\sigma = 0.20$ dB, and we set the detection threshold of $4\sigma = 0.80$ dB. Since an inserted loss of 1.20-dB exceeded the threshold, LPM successfully detected the 1.20-dB loss anomaly and potentially localizes a 0.80-dB loss. These results demonstrate the feasibility of LPM for use in system operations.

6. Summary

We have reviewed the fundamentals and recent advancements in LPM. Recent intensive efforts have led to significant progress towards its practical implementation, such as a precise LPM that closely matches OTDR, the feasibility demonstration at operational launch power, and adapting LPM for use with commercial transponders. To achieve more reliable performance for deployment, future research should include (i) improving noise and distortion robustness for enhanced accuracy at operational optical power levels, (ii) developing lightweight algorithms, (iii) enhancing functionality for monitoring a wider range of link parameters.

References

- [1] T. Tanimura et al., “Fiber-longitudinal anomaly position identification over multi-span...,” *J. Lightw. Technol.*, **38**(9), 2726–2733, 2020.
- [2] T. Sasai et al., “Digital longitudinal monitoring of optical fiber communication link,” *J. Lightw. Technol.* **40**(8), 2390–2408, 2022.
- [3] T. Sasai et al., “Performance limit of fiber-longitudinal power profile estimation methods,” *J. Lightw. Technol.* **41**(11), 3278–3289, 2023.
- [4] T. Sasai et al., “Linear least squares estimation of fiber-longitudinal optical power profile,” *J. Lightw. Technol.* (early access), 2023.
- [5] A. May et al., “Longitudinal power monitoring over a deployed 10,000-km link for submarine systems,” *OFC*, Tu2G.3, 2023.
- [6] C. Hahn, et al., “Localization of reflection Induced multi-path-interference...,” *OFC*, Th1C.3, 2022.
- [7] T. Sasai et al., “A generalized method for fiber-longitudinal power profile estimation,” *ECOC*, Tu.A.2.6., 2023.
- [8] M. Sena, et al., “Advanced DSP-based monitoring for spatially resolved...,” *J. Lightw. Technol.*, **41**(3) 989–998, 2023.
- [9] M. Eto et al., “Location-resolved PDL monitoring with Rx-side digital signal processing...,” *OFC*, Th1C.2, 2022.
- [10] M. Takahashi et al., “Experimental demonstration of monitoring PDL value and location...,” *ECOC*, P14, 2023.
- [11] L. Andrenacci et al., “PDL localization and estimation through linear least...,” *IEEE Photon. Technol. Lett.*, **35**(24), 1431–1434, 2023.
- [12] J. Chang et al., “Demonstration of longitudinal power profile estimation using Commercial Transceivers...,” *ECOC*, Tu.A.2.2, 2023.
- [13] C. Hahn et al., “On the spatial resolution of location-resolved performance monitoring by correlation method,” *OFC*, W1H.3, 2023.
- [14] R. Hui et al., “Measurement of total and longitudinal nonlinear phase shift...,” *J. Lightw. Technol.*, **40**(21), 7020–7029, 2022.
- [15] P. Serena et al., “Locating fiber loss anomalies with a receiver-side monitoring algorithm exploiting cross-phase...,” *OFC*, W1H.3, 2023.
- [16] I. Kim et al., “Multi-channel longitudinal power profile estimation,” *ECOC*, Tu.A.2.4, 2023.